# Multi-magnetic properties of a novel SCO [Fe(3-OMe-Sal$_2$trien)][Fe(tdas)$_2$]·CH$_3$CN salt

Nataliya Spitsyna,*[a] Nikolay Ovanesyan,[a] Maxim Blagov[a,e], Vladimir Krapivin,[a] Anatolii Lobach,[a] Alexei Dmitriev,[a] Sergey Simonov,[b] Leokadiya Zorina,[b] Luca Pilia,[c] Paola Deplano,[d] Alexander Vasiliev,[e,f] Olga Maximova,[e,h] and Eduard Yagubskii[a]

[a] Dr. N. Spitsyna, Dr. N. Ovanesyan, M. Blagov, V. Krapivin, Dr. A. Lobach, Dr. A. Dmitriev, Prof. E. Yagubskii
Institute of Problems of Chemical Physics, RAS, Chernogolovka, MD 142432, Russia
E-mail: spitsina@icp.ac.ru
[b] Dr. S. Simonov, Dr. L. Zorina
Institute of Solid State Physics, RAS, Chernogolovka, MD 142432, Russia
[c] Prof. L. Pilia
Dipartimento di Ingegneria Meccanica, Chimica e dei Materiali, Università di Cagliari, via Marengo 2, I09123, Cagliari, Italy
[d] Prof. P. Deplano
Dipartimento di Fisica, INSTM Research Unit, University of Cagliari, I-09042, Monserrato, Cagliari, Italy
[e] Prof. A. Vasiliev, Dr. O. Maximova, M. Blagov,
Lomonosov Moscow State University, Moscow 119991, Russia
[f] Prof. A. Vasiliev
National Research South Ural State University, Chelyabinsk 454080, Russia
[h] Dr. O. Maximova
National University of Science and Technology "MISIS", Moscow 119991, Russia

Supporting information for this article is given via a link at the end of the document.

**Abstract:** The multi-magnetic salt [Fe(3-OMe-Sal$_2$trien)][Fe(tdas)$_2$]·CH$_3$CN (**1**) has been prepared and fully characterized by a variety of methods. The crystal structure of **1,** determined at 150, 297 and 350 K, consists of alternating layers composed by a parallel arrangement of the chains of isolated π-π coupled cation pairs of [Fe(3-OMe-Sal$_2$trien)]$^+$ and anion pairs of [Fe(tdas)$_2$]$^-$. The complex magnetic behavior of this salt is consistent with the sum of the contributions from spin-crossover (SCO) cations and strong antiferromagnetically (AFM) coupled dimeric [Fe(tdas)$_2$]$_2^{2-}$ anions. The observed gradual thermally induced spin transition ($T_{1/2}$=195 K) is relatable to the cation exhibiting disordering of ethylene (-CH$_2$-CH$_2$-) groups between two conformers with a narrow thermal hysteresis of 6 K. The *dc* magnetization measurements and $^{57}$Fe Mössbauer spectroscopy at room temperature are in excellent agreement between $\gamma_{HS}$(%) value and ratio of disordering of ethylene groups obtained from X-ray analysis. Mössbauer spectra at 80 K and 296 K indicate a spin transition between S=1/2 and S=5/2 for the iron(III) saltrien-cation and confirms S=3/2 for the [Fe$^{III}$(tdas)$_2$]$^-$ anion. The experimental results are supplemented with a theoretical Density Functional Theory (DFT) analysis.

## Introduction

Spontaneous assembly of molecules exhibiting magnetic properties into non-covalently linked stable aggregates, is a promising approach to obtain multi-magnetic *"smart"* materials, of current interest for application in electronic devices.[1-9] In this context, spin-crossover (SCO) Fe(II/III) coordination complexes carrying of magnetic "bi-stability" at the molecular level, represent one of the promising building blocks for such materials. In these aggregates switching between the low-spin (LS) and high-spin (HS) states, induced by variation of temperature and/or pressure and by light irradiation, leads to distinctive changes in magnetism, colour and structure.[2] In the case of iron(III) ($d^5$), reversible SCO is associated with the switching between low-spin (LS, S=1/2) and high-spin (HS, S=5/2) states of metal center.[10, 11] SCO Fe(III) octahedrically coordinated complexes with saltrien-type ligands (X-Sal$_2$trien = hexadentate N$_4$O$_2$ Schiff bases are products of condensation of triethylenetetramine with salicylaldehyde derivatives) are actively used as molecular building blocks in the synthesis of metal–organic/inorganic hybrid materials,[12] switchable molecular conductors,[13] multi-magnetic compounds.[14-15] The spin transitions in [Fe(3-/5-X-Sal$_2$trien)]$^+$ cations (X different substituents in salicylaldehyde) are highly sensitive to supramolecular packing, which is affected by the nature of counterions and solvate molecules. Simplicity of synthesis, a wide possibility of ligand tuning and stability of these cationic complexes make them very attractive candidates as building blocks of multi-magnetic materials.[12(a, d, e)-19] In most SCO compounds based on [Fe(Sal$_2$trien)]-complexes, a gradual incomplete spin transition is observed without any hysteresis. However, the salt [Fe(Sal$_2$trien)][Ni(dmit)$_2$] (dmit = 2-thioxo-1,3-dithiole-4,5-dithiolate) demonstrates an abrupt spin transition behavior with a wide thermal hysteresis loop ($\Delta T_{SCO}$ = 30 K). Exchange interactions between the iron(III) centers of cations and the formally Ni$^{3+}$ ions of the anion were not observed.[13a] Apparently, the abrupt SCO in this salt is favored by the crystal packing.[20] Relationship between hysteresis loop and intermolecular interactions has been reported recently for the salt [Fe(3-OMe-Sal$_2$trien)][Au(dmit)$_2$].[21] Remarkably, it was shown that molecular interactions determine the geometry of the complexes, orientation of ethylene groups, and effect the iron(III) spin state of the [Fe(3-/5-X-Sal$_2$trien)]$^+$ cationic complexes.[21, 22] These findings point out that the counterion plays a crucial role in Fe-saltrien-type cationic complexes to try to reach a SCO behavior. In this contest, the magnetic and structural features of the [Fe(tdas)$_2$]$^-$ complex (tdas = 1,2,5-thiadiazole-3,4-dithiolato) seemed to us attractive to employ this anion as components of multifunctional molecular solids.[23-26] The [Fe(tdas)$_2$]$^-$ anion with a distorted square-pyramidal coordination sphere is present in most crystal structures as a centrosymmetric dimer formed by metal-sulfur (Fe···S) bonds through overlap of $d_{z^2}$ orbitals of iron and $p_z$ orbitals of apical sulfurs, where the apical Fe–S distance

is longer than the equatorial ones. In the anion, the iron(III) ($d^5$) ions exhibits intermediate spin (IS) state (S=3/2). Furthermore, strong antiferromagnetic exchange is realized between the two magnetic centers.[12b, 12c, 24-26] An unusual "reentrant" magnetic behavior associated with the increase of magnetization ($\chi_p$) in the ranges 190–250 K range at heating and 230–180 K at cooling has been reported for the ($n$Bu$_4$N)[Fe(tdas)$_2$] ($n$Bu$_4$N = tetrabutylammonium) salt.[24]

On the basis of these short introductory notes [Fe(3-OMe-Sal$_2$trien)]$^+$ is expected to behave as a SCO cation, where the electron-donating (3-OMe-) substituent should weaken the ligand field by enhancing ligand-metal π-donation and stabilizing the HS state of the complex.[27,28] This, when the cation is combined with [Fe(tdas)$_2$]$^-$ (Figure 1), can contribute to the shift $T_{SCO}$ in the area of "reentrant" magnetic behavior observed in the ($n$Bu$_4$N)[Fe(tdas)$_2$] salt, and possibly might entail a new unusual magnetic properties. In addition, the structural changes in [Fe(3-OMe-Sal$_2$trien)]$^+$ as a result of SCO, can lead to significant restructuring of the crystal lattice affecting the spin state of this cation.[22, 27, 28]

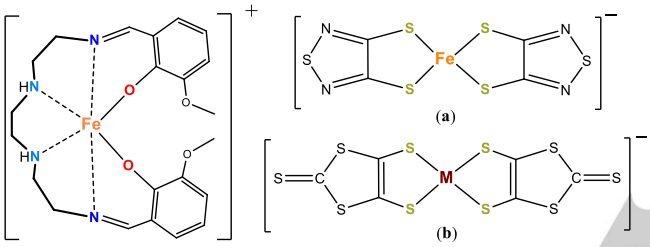


**Figure 1.** Scheme of the cation [Fe(3-OMe-Sal$_2$trien)]$^+$ (left) and anions [Fe(tdas)$_2$]$^-$ (right, **a**); [M(dmit)$_2$]$^-$ (M=metal cation) (right, **b**). Ethylene groups of 3-OMe-Sal$_2$trien$^{2-}$ ligand are highlighted in bold.

Understanding the role of interactions in salts of iron(III) sal$_2$trien cationic complexes with anionic metal-dithiolenes in affecting their properties overcomes the interest in material field. Currently these salts are employed as synthetic models in bioorganic chemistry for modeling active centers in iron-containing proteins and heme iron enzymes.[29]

With the view to contribute in elucidating these important issues, we have combined [Fe(3-OMe-Sal$_2$trien)]$^+$ and [Fe(tdas)$_2$]$^-$ successfully obtaining the two different magnetic subsystems in the same crystal lattice of the salt [Fe(3-OMe-Sal$_2$trien)][Fe(tdas)$_2$]·CH$_3$CN (**1**).

Here we report the synthesis of **1** and a joint experimental-computational study, based on X-ray analysis, *dc* magnetization measurements at variable temperature and $^{57}$Fe Mössbauer spectroscopy, supplemented with a theoretical DFT analysis.

## Results and Discussion

### Synthesis and characterization

The salt [Fe(3-OMe-Sal$_2$trien)][Fe(tdas)$_2$]·CH$_3$CN (**1**) was synthesized by the metathesis reaction of ($n$Bu$_4$N)[Fe(tdas)$_2$] (**2**)[23b] and [Fe(3-OMe-Sal$_2$trien)]NO$_3$·H$_2$O (**3**)[30] in acetonitrile (CH$_3$CN) at room temperature (see experimental section). Crystals of **1**, suitable for X-ray diffraction, were obtained by slow diffusion of acetone solution of ($n$Bu$_4$N)[Fe(tdas)$_2$] into acetonitrile solution of [Fe(3-OMe-Sal$_2$trien)]NO$_3$·H$_2$O (see photo in the Supporting Information (SI) Figure S1). These crystals are stable in air, and can be stored under ambient conditions.

The purity of the complexes **1**-**3** and their solvation state was checked by analytical methods. The elements proportion Fe:S in **1** was estimated by the electron-probe X-ray microanalysis (*EPMA*).

The thermogravimetric analysis of **1** revealed a mass loss of 4.72% in the temperature range 122-214 °C (out of the temperature range of magnetic measurements of **1**, see related section) that is in agreement with the loss of one CH$_3$CN molecule of lattice (calcd. 4.76%) (SI Figure S2).

The phase purity of **1**, taken for magnetic measurements, was confirmed by the powder X-ray diffraction (*PXRD*) pattern in the 2θ range from 2° to 45° and compared to the simulated powder diffractogram from the X-ray structural data (SI Figure S3).

Experimental *ATR FT-IR* absorbance spectra for the compounds **1**-**3** and calculated IR vibration frequencies for the AFM coupled dimer [Fe(tdas)$_2$]$_2^{2-}$ are shown in Figure 2. IR spectrum of **1** is the superposition of characteristic modes of [Fe(3-OMe-Sal$_2$trien]$^+$ cation and dimeric [Fe(tdas)$_2$]$_2^{2-}$ anion with negligible shifts relative to the absorption bands of the precursors **2** and **3**. Comparison of selected DFT calculated and experimental **1**, **2** IR vibration modes for the dimeric [Fe(tdas)$_2$]$_2^{2-}$ is in a good agreement (Figure 2, Table S1 in SI). Graphical representations of selected calculated IR vibrational modes for the dimer [Fe(tdas)$_2$]$_2^{2-}$ are depicted in SI Figure S4.

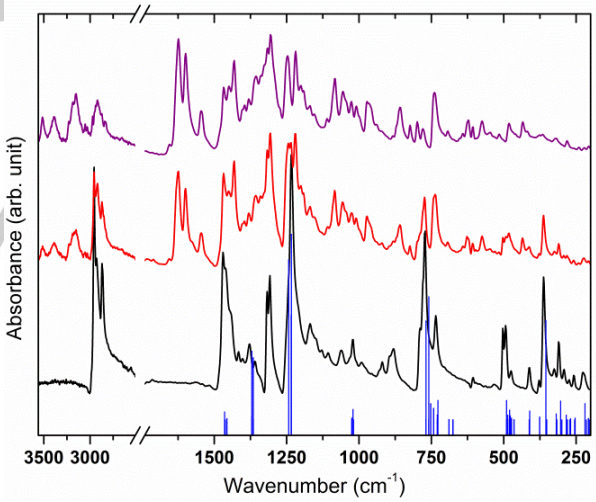


**Figure 2.** Experimental *ATR FT-IR* absorption spectra for the **1** (purple line), **3** (red line) and **2** (black line) at T=296 K, without preliminary sample preparation. DFT calculated IR vibration frequencies for the dimeric [Fe(tdas)$_2$]$_2^{2-}$ (blue bars). TPSSh functional with 6-311++G(d,p) basis set was used.

Comparison of DFT calculated for the two conformers of [Fe(3-OMe-Sal$_2$trien)]$^+$ cation and experimental **1**, **3** IR spectra are shown in SI Figure S5. The observed multiplicity of N-H(st) and C=N(st), may be relatable to changes in their environment in molecules of different Fe(III) spin states (see X-ray and magnetic properties).[30] The intensity change and broadening of the absorption lines of N-H stretching modes (νN-H) at 3514 cm$^{-1}$, 3054 cm$^{-1}$ and 1578 cm$^{-1}$ and C=N bending modes (δC=N) at 1623,5 cm$^{-1}$ for **1** may be due to the presence of two conformers of saltrien-cation in HS/LS states as compared to **3** in LS state (see below) (SI Figures S5 and S6, Tables S2 and S3).

### Single crystal X-ray structure

Single crystal X-ray diffraction experiments were carried out at 150, 297 and 350 K, which confirmed the molecular structure of [Fe(3-OMe-Sal$_2$trien)][Fe(tdas)$_2$]·CH$_3$CN (**1**) (SI Table S4). Complex **1** crystallizes in the triclinic space group P $\bar{1}$. Asymmetric unit includes the [Fe(tdas)$_2$]$^-$ anion, the [Fe(3-OMe-Sal$_2$trien)]$^+$ cation and one solvent acetonitrile molecule, all in general positions (Figure S7). An ORTEP drawing of **1** is shown in Figure 3; key bond distances and angles are listed in Table 1.

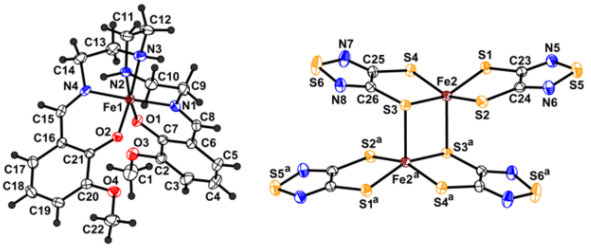


**Figure 3.** Cation of [Fe(3-OMe-Sal$_2$trien)]$^+$ (left) and anion dimer of [Fe(tdas)$_2$]$_2^{2-}$ (right) with atom labels. Symmetry code: (a) (2-*x*, -*y*, -*z*).

The structure has a layered packing with alternation of cation [Fe(3-OMe-Sal$_2$trien)]$^+$ and anion [Fe(tdas)$_2$]$^-$ layers along *c*-direction (Figure 4). Solvent molecules are located at the interface of cation and anion layers. Anions are non-planar with dihedral angle between two Fe-tdas planes of 25.96° at 150 K, which decreases to 19.84° at 297 K and 19.19° at 350 K. The anions form centrosymmetric dimers [Fe(tdas)$_2$]$_2^{2-}$ through Fe-S (out-of-plane) bond of 2.4679(6)Å at 150K, which increases to 2.4771(8)Å at 297K and 2.4796(7)Å at 350K (Figure 3). Similar temperature changes in angles and bonds were noted for (*n*Bu$_4$N)[Fe(tdas)$_2$], as described earlier[24, 31]: 16.96° and 2.483(1)Å at 150 K; 14.75° and 2.501(2)Å at 298K.

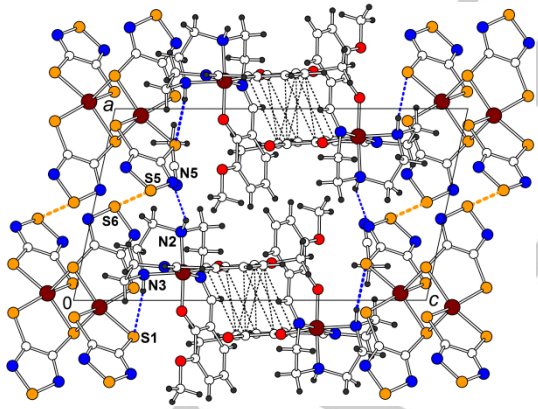


**Figure 4.** Projection of the structure **1** (150 K) along *b* direction. Intermolecular contacts S···S (yellow dashed lines), C···C (< 3.6 Å, black dotted lines) and hydrogen N-H···N/S bonds (blue dashed lines) are shown.

The iron(III) ions have the square-pyramidal configuration in dimeric anion, as generally found.[25] The Fe-S (in plane) distances of tdas-anion in **1** are not equal and range from 2.2445(7)Å to 2.2831(6)Å at 150 K, from 2.2360(8)Å to 2.2765(8)Å at 297K and from 2.2357(7)Å to 2.2797(7)Å at 350 K, what is also a consequence of the dimerization.[25] The interdimer contacts between the terminal sulfur atoms are found in the anion layer of **1** (Figure 4) with S···S distance of 3.2446(9), 3.315(1) and 3.360(1)Å at 150, 297 and 350 K, respectively.

**Table 1.** Selected bond lengths (Å) and angles (°) in salt **1** at different temperatures.

| Parameter | 150 K | 297 K | 350 K |
|---|---|---|---|
| Fe1 O2 | 1.880(1) | 1.896 (2) | 1.899(2) |
| Fe1 O1 | 1.881(2) | 1.897(2) | 1.902(2) |
| Fe1 N4 | 1.930(2) | 2.064(2) | 2.095(2) |
| Fe1 N1 | 1.945(2) | 2.078(3) | 2.112(2) |
| Fe1 N2 | 2.014(2) | 2.126(3) | 2.159(2) |
| Fe1 N3 | 2.012(2) | 2.144(3) | 2.177(2) |
| Fe2 S2 | 2.2445(7) | 2.2439(8) | 2.2448(7) |
| Fe2 S1 | 2.2514(6) | 2.2360(8) | 2.2357(7) |
| Fe2 S4 | 2.2547(7) | 2.2527(8) | 2.2557(8) |
| Fe2 S3 | 2.2831(6) | 2.2765(8) | 2.2797(7) |
| Fe2 S3$^a$ | 2.4679(6) | 2.4771(8) | 2.4796(7) |
| O2 Fe1 O1 | 96.56(7) | 102.04(9) | 103.27(8) |
| O2 Fe1 N4 | 93.00(7) | 88.26(9) | 87.44(7) |
| O1 Fe1 N4 | 88.00(7) | 91.18(9) | 92.14(8) |
| O2 Fe1 N1 | 88.49(7) | 91.94(9) | 92.78(8) |
| O1 Fe1 N1 | 93.40(7) | 88.45(10) | 87.54(9) |
| N4 Fe1 N1 | 177.83(8) | 179.60(10) | 179.65(9) |
| O2 Fe1 N2 | 89.53(7) | 92.13(10) | 92.30(8) |
| O1 Fe1 N2 | 173.30(7) | 161.15(11) | 159.02(9) |
| N4 Fe1 N2 | 94.47(8) | 101.73(10) | 102.66(8) |
| N1 Fe1 N2 | 83.95(8) | 78.60(11) | 77.60(9) |
| O2 Fe1 N3 | 173.57(7) | 162.78(9) | 160.27(9) |
| O1 Fe1 N3 | 89.09(7) | 89.48(10) | 90.02(9) |
| N4 Fe1 N3 | 84.11(8) | 78.65(11) | 77.40(9) |
| N1 Fe1 N3 | 94.25(8) | 101.21(11) | 102.43(9) |
| N2 Fe1 N3 | 84.98(8) | 79.80(10) | 78.99(9) |
| S2 Fe2 S1 | 91.15(2) | 91.32(3) | 91.50(3) |
| S2 Fe2 S4 | 158.05(3) | 155.08(4) | 154.58(3) |
| S1 Fe2 S4 | 83.80(2) | 85.28(3) | 85.58(3) |
| S2 Fe2 S3 | 85.02(2) | 84.62(3) | 84.51(3) |
| S1 Fe2 S3 | 158.62(3) | 163.88(4) | 165.16(3) |
| S4 Fe2 S3 | 91.93(2) | 91.84(3) | 91.90(3) |
| S2 Fe2 S3 | 101.85(2) | 102.53(3) | 102.81(3) |
| S1 Fe2 S3 | 104.68(2) | 100.49(3) | 99.61(3) |
| S4 Fe2 S3 | 100.09(2) | 102.37(3) | 102.57(3) |
| S3 Fe2 S3$^a$ | 96.68(2) | 95.62(3) | 95.22(2) |

Symmetry code: (a) (2-*x*, -*y*, -*z*)

The value at 150 K is somewhat greater than 3.237(2)Å determined for similar contact in (BETS)$_2$[Fe(tdas)$_2$]$_2$ salt at 160 K.[12c] One should note such key parameters as the φ angle (Fe(2)-S(3)-Fe(2)$^a$) and interlayer distance (Fe(2)-S(3)$^a$), which play an important role in the value of antiferromagnetic exchange coupling constant (*J*) between the iron centers (Figure 3).[32a]

In the cationic layer, [Fe(3-OMe-Sal$_2$trien)]$^+$ form isolated π-π coupled pairs with a lot of several shortened C···C contacts (less lower than sum of van der Waals radii, 3.6 Å) (Figure 4), that should decrease the SCO cooperative effect. Moreover, it may be a reason of arising AFM exchange between two iron(III) centers. AFM interactions in π-π coupled pairs of [Fe(3-OMe-Sal$_2$trien)]$^+$ cations were also observed earlier in [Fe(3-OMe-Sal$_2$trien)][Au(dmit)$_2$] salt, where SCO phenomenon does not occur: while the HS state is stabilized.[21] In the present case, thermal SCO behavior is observed, as expected for the ligand conformation of cation. It is well known that upon the LS to HS transition Fe-N$_{am}$, Fe-N$_{im}$ and Fe-O bond lengths increase as

well as a dihedral angle α between two phenoxide planes of the cation,[28] and the central Fe octahedron becomes more distorted. In our recent work[22] we found that conformations of the ethylene groups in the saltrien-type cations also gives a good response on the Fe(III) spin state. At 150 K the geometry of $FeN_4O_2$ octahedron in **1** (Table 1) and the angle α=79.77° (α<90°) indicate LS state of iron(III) in SCO cation. The ligand conformations also correspond to Δ(λδλ) LS conformer (SI Figure S8).[32b] At room temperature, the iron-ligand bonds increase by ~6.5% for Fe-$N_{am}$, ~6.8% for Fe-$N_{im}$ and ~0.9% for Fe-O compare to 150 K structure, as well the α angle increases as well up to 80.90°. The ethylene groups are disordered between two different conformations with 0.72:0.28 ratio pointing to presence of 72% of Δ(λλλ) HS and 28% of Δ(λδλ) LS conformers, respectively. At 350K, the iron-ligand bonds continue to increase until ~8.2% for Fe-$N_{am}$, ~8.6% for Fe-$N_{im}$ and ~1.1% for Fe-O compare to 150 K structure, likewise the α angle increases up to 82.34° (still α<90° under the crystal packing influence). An attempt to refine disordering of ethylene groups at 350 K gives less than 10% of the Δ(λδλ) LS conformer (the final cif-file does not contain this information). It can be expected that the $[Fe(3\text{-}OMe\text{-}Sal_2trien)]^+$ cation has only HS Fe(III) at T > 350K.

The cation and anion layers in **1** interact by hydrogen bonding from N-H donors of the cation (Figure 4). At 150 K, geometry of N-H···N bond: H···N = 2.24Å, N···N = 3.082(2)Å, N-H···N angle = 141.4(1)°; N-H···S bond: H···S = 2.67Å, N···S = 3.666(2)Å, N-H···S angle = 170.5(1)°. At 350 K, N-H···N bond slightly shortens, while N-H···S bond disappears. The $CH_3CN$ solvent molecule is in a dense environment of three cations and two anions interacting with them by C···C, C···S, C-H···N/O contacts.

**Magnetic properties and $^{57}$Fe Mössbauer spectroscopy**

The *dc* magnetic susceptibility was measured in a temperature range of 2–350 K at B = 0.1 T (the temperature was changed by a rate of 2 K/min) at heating and cooling modes, the corresponding temperature dependences of $\chi T$ product are shown in Figure 5.

The coexistence of $[Fe(3\text{-}OMe\text{-}Sal_2trien)]^+$ SCO cations and dimeric $[Fe(tdas)_2]_2^{2-}$ anions in crystal structure leads to sophisticated temperature dependence of χT. Starting with the χT value of 3.93 $cm^3 \cdot K \cdot mol^{-1}$ at 300 K, the magnetic susceptibility gradually decreases down to 1.08 at 50 K (Figure 5). Furthermore, drastic decrease of χT values down to 0.52 $cm^3 \cdot K \cdot mol^{-1}$ at 2 K was also observed below 50 K. Similarly to cooling process, the χT values of heating process increased up to 4.28 $cm^3 \cdot K \cdot mol^{-1}$ at 350 K, with a small hysteresis loop of about 6 K between ca. 94 and 200 K. This is a typical behaviour for an iron(III) SCO compound (SI Figure S9). One can conclude from the analysis of X-ray data of **1** at various temperatures that the SCO behavior of the $[Fe(3\text{-}OMe\text{-}Sal_2trien)]^+$ cations takes place between low-spin (S=1/2) and high-spin (S=5/2) states. The dependence of χT *vs* T is expected to be the sum of the contributions of the anionic ($\chi_D T$) and cationic ($\chi_{LH} T$) magnetic subsystems: AFM coupled dimerized $[Fe(tdas)_2]^-$ anions with S=3/2 and $[Fe(3\text{-}OMe\text{-}Sal_2trien)]^+$ cations with S=1/2 or S=5/2. The cation–anion magnetic interactions are assumed to be weak. On the basis of the collected experimental data, we propose here a model resulting in satisfactory agreement with the observed trend behavior of magnetic susceptibility for the multi-magnetic salt $[Fe(3\text{-}OMe\text{-}Sal_2trien)][Fe(tdas)_2]\cdot CH_3CN$. To describe the magnetic behavior of $[Fe(3\text{-}OMe\text{-}Sal_2trien)]^+$ cations, we used Equation **1**, which was proposed to analyze the magnetic properties of ferric N,N-dialkyldithiocarbamate complexes $Fe(S_2CNR_2)_3$, demonstrating a gradual spin transition.[33,34]

$$\chi_{\mathrm{LH}} T = \frac{1}{8}\frac{0.75 g_1^{\,2} + 8x^{-1}(1+e^{-3x/2}) + 105Ne^{-(1+(E/\xi))x}}{1+2e^{-3x/2}+3Ne^{-(1+(E/\xi))x}} \qquad \text{Eq. } \mathbf{1}$$

where $g_1$ is the spectroscopic splitting factor applicable to the $^2T_2$ (LS, S=1/2) state, $x = \xi/k_BT$, $\xi$ – one-electron spin-orbital coupling constant, $T$ is the temperature in Kelvin, $E$ is the separation between zero-points levels of the two states and $N$ is the ratio of the molecular vibrational partition functions for HS and LS states. The $g_1$-parameter was fixed at 2.00.[4, 21, 33, 34] Moreover, $\xi$-parameter was also fixed at 370 $cm^{-1}$ (532.4 K) according to Ewald's value for $Fe(S_2CNR_2)_3$ complexes.[33] The $N$-parameter was set equal to 10 since this value is appropriate for most of iron(III) complexes.[33]

Concerning the analysis of the magnetic properties of $[Fe(tdas)_2]_2^{2-}$ dimers, earlier Awaga *et al.*[24] demonstrated that the magnetic behavior of dimerized $[Fe(tdas)_2]^-$ anions with antiferromagnetic coupling can be described by Equation **2**, which is applicable for our case.

$$\chi_D T = \frac{N_A g_2^{\,2} \mu_B^2}{k_B}\frac{e^{-2J_2/k_BT}+5e^{-6J_2/k_BT}+14e^{-12J_2/k_BT}}{1+3e^{-2J_2/k_BT}+5e^{-6J_2/k_BT}+7e^{-12J_2/k_BT}} \qquad \text{Eq. } \mathbf{2}$$

where $g_2$ is the isotropic Landé factor for Fe(III) in the intermediate state (S=3/2), $N_A$, $\mu_B$ and $k_B$ are Avogadro, Bohr magneton and Boltzmann constants and $J_2$ is the intradimer exchange interactions parameter. The $g_2$-parameter was fixed at 1.88 as reported by Awaga *et al.*[24]

The experimental data cannot be described by the sum of Eq. **1** and Eq. **2** only, since Eq. **1** presumes full transformation of $Fe^{3+}$ from high-spin state (S = 5/2) to low-spin state (S = 1/2). We have to suggest that a residual HS fraction exists in the sample of salt **1** at low temperatures.[21] This hypothesis is reasonable since the electron-donating 3-OMe substitutions of saltrien-ligand stabilize the high-spin states of the SCO cation.[28] A gradual decrease in χT values below 50 K may originate from either the SCO conversion of HS Fe(III) species or the AFM interaction between paramagnetic centers.[21, 35] In our case, we do not observe a χT plateau typical for saltrien-complexes down to helium temperature.[21, 28] It means that SCO process and AFM exchange of residual HS fraction coexist.

Thus, the term

$$\chi_{C-W} T = \frac{C_{HS}\cdot T}{T-\theta} \qquad \text{Eq. } \mathbf{3}$$

with $C_{HS}$=4.377 $cm^3 \cdot K \cdot mol^{-1}$ representing the contribution (ρ)[21, 35, 36, 37] of residual HS faction of SCO cation should be taken into account to describe data in the lowest temperature range. Overall, the experimental χT can be fitted by Eq. **4**.

$$\chi T = \chi_{LH} T \cdot (1-\rho) + \chi_{C-W} T \cdot \rho + \chi_D T \qquad \text{Eq. } \mathbf{4}$$

The first term reflects the magnetic behavior of iron(III) SCO cations, the second term reflects the magnetic behavior of

residual HS fraction and the third term accounts for the impact from magnetically coupled dimers of Fe(III) (S=3/2) in anionic layer.

The fitting curve and individual contributions from two magnetic subsystems are shown in Figure 5. The best fit of experimental data by Eq. **4** was obtained with the set of parameters presented in Table 2.

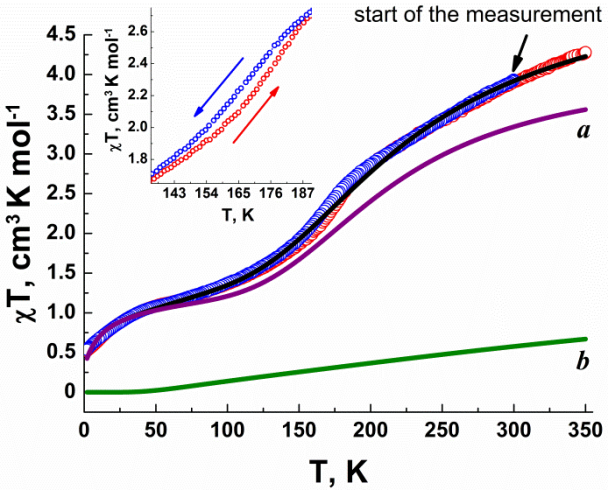


**Figure 5.** Temperature dependences of χT product at heating (red circles, ○) and cooling (blue circles, ○) modes. Black solid line is the fit of experimental data by sum of two contributions. The purple (***a***) and green (***b***) lines represent the calculated magnetic behavior of spin-crossover cations [Fe(3-OMe-Sal$_2$trien)]$^+$ (sum of Eqs. **1** and **3**) and dimerized [Fe(tdas)$_2$]$^-$ anions (Eq.**2**), respectively. The inset to the figure shows the enlarged region of hysteresis loop. The arrows indicate the direction of temperature sweep.

**Table 2.** Parameters of the best fit of experimental data of $\chi T$ vs. $T$ according to Equation **4**.

| Parameter | [Fe(3-OMe-Sal$_2$trien)]$^+$ | Parameter | [Fe(tdas)$_2$]$^-$ |
|---|---|---|---|
| $g_1$ | 2 (fixed) | | |
| ξ, K | 532 (fixed) | $g_2$ | 1.88 (fixed) |
| $E$[b], K | 262 | | |
| $N$ | 10 (fixed) | | |
| ρ[b] | 0.184 | $J_2/k_B$[a,b], K | 99.47±0.19 |
| $\theta$[b], K | -12 | | |

[a] The "–" sign of AFM exchange was taken into account in the equation **2**.
[b] The $E$, $\rho$, $J_2$ and parameter $\theta$ were calculated within the confines of $E$, $\rho$, $J_2$ > 0 and $\theta$ < 0, respectively.

The $E$ value is very sensitive to variations in the ligands and as a consequence to changes in the crystal forces.[33] Obtained $E$ value is equal to 262 K. It means that the $^6A_1$ (HS) state lies the higher than $^2T_2$ (LS) state.[33] Deviations from ordinary LS/HS behavior are seen only when $|E|/\xi$ < 1.[34] For [Fe(3-OMe-Sal$_2$trien)]$^+$ SCO cation in the salt **1**, a reasonable $|E|/\xi$ value equal to ~0.5 has been found. In addition, on the basis of the fitted ρ-parameter, the amount of S = 5/2 residual HS fraction was estimated as ~ 18.4 %. Note, a value for [Fe(3OMe-Sal$_2$trien)][Au(dddt)$_2$]·CH$_3$CN salt has been estimated as ~ 20%.[21] Probably, the existence of residual HS fraction is characteristic of SCO compounds based on [Fe(3-OMe-Sal$_2$trien)]$^+$ cation. A negative value of the Weiss temperature θ = −12 K evidences weak AFM interaction between magnetic centers in salt **1**. One of the possible exchange paths can be ascribed to the presence of π-staking interactions of molecules pair in the cationic layer.

The negative sign of the exchange integral $J_2/k_B$=–99.47±0.19 K (Eq. **2**) between the iron(III) centers of [Fe(tdas)$_2$]$_2^{2-}$ dimer indicates the AFM character of magnetic interactions in accordance with DFT calculations (see below).

The calculated χT value for contribution of SCO cation (curve ***a*** in Figure 5) gradually increases and reaches the value of 3.32 cm$^3$·K·mol$^{-1}$ at 296 K and 3.56 cm$^3$·K·mol$^{-1}$ at $T$=350 K, which corresponds to the mixture states with $\gamma_{HS}$(calc.)=74% and $\gamma_{HS}$(calc.)=80%, respectively. The $\gamma_{HS}$(calc.) values were calculated according to formula:

$$\gamma_{HS}(calc.) = (\frac{\chi_{LH}T - 0.375}{4.377 - 0.375}\cdot(1-\rho)+\rho)\cdot 100\%$$

This is in a good agreement with results obtained from X-ray crystal structure analysis. The iron(III)-ligand bond lengths and the characteristic angle α of the SCO [Fe(3-OMe-Sal$_2$trien)]$^+$ cation increase with temperature rises in agreement with the SCO process. The occupation ratio of Δ(λλλ) HS and Δ(λδλ) LS state conformers is 72% and 28% at 297 K, in agreement with magnetic data $\gamma_{HS}$(calc.)=75%. The fraction of Δ(λλλ) HS state conformer at 350 K of 90% is somewhat higher than $\gamma_{HS}$(calc.)=80%. This allows concluding that ethylene groups disordering relates to cooperative structural effects and it is strongly dependent on crystal packing features. According to the simulated curve ***a*** (Figure 5), the spin transition temperature $T_{1/2}$, where $\gamma_{HS}$ is 50%, is equal to 195 K that is above the middle of hysteresis loop *ca.* 168 K (SI Figures S9 and S10). The first derivative curve of the magnetic susceptibility data of **1** illustrates a one-step SCO behavior with the maximum rate of $\chi T$ change at ~170 K (cooling mode) and ~178 K (heating mode) (SI Figure S11). The $\chi T$ value for **1** at 350 K is clearly lower than the expected value for the HS Fe(III) state (S=5/2). The $\chi T$-$T$ plot of **1** did not reach the plateau region, even at 350 K (Figure 5), the LS→HS transition is considered incomplete. The calculated temperature of complete spin-state switching is estimated at 3256 K (SI Figure S10).

Compound **1** was further characterized by $^{57}$Fe zero-field Mössbauer spectroscopy at 80K and 296 K (Figure 6). This technique was applied to confirm the *dc* magnetic measurements and to support the determination the $\gamma_{HS}$(calc.) (%) value from the ratio of disordered ethylene groups of the cation obtained from X-ray analysis at room temperature. Moreover, an analysis of the Mössbauer spectra provides insight into which of the Fe(III) ions present in the multi-magnetic salt **1** undergo SCO. Attribution of spectral components for the salt [Fe(3-OMe-Sal$_2$trien)][Fe(tdas)$_2$]·CH$_3$CN was carried out in line with the measurements of single-component in iron(III) complexes ($n$Bu$_4$N)[Fe(tdas)$_2$] (S=3/2) and [Fe(3-OMe-Sal$_2$trien)]NO$_3$·H$_2$O (S=1/2) (SI Figure S12 and S13).

The spectrum obtained at 80 K contains two quadrupole doublets (see Figure 6). The first doublet has Mössbauer parameters characteristic of LS iron(III) saltrien-complex, namely isomer shift $\delta$=0.23(1) mm/s, quadrupole splitting $\Delta E_Q$=2.53(1) mm/s and line width $\Gamma$=0.31(1) mm/s.[33, 38, 39] The second doublet with $\delta$=0.33(1) mm/s, $\Delta E_Q$=3.02(1) mm/s and $\Gamma$=0.33(1) mm/s is typical of [Fe(tdas)$_2$]$^-$ anion in the IS state.[26]

The 296 K Mössbauer spectrum of salt **1** shows three quadrupole doublets (Figure 6). The first two quadrupole

doublets have parameters corresponding to HS (S=5/2) Fe(III) ($\delta$=0.35(1) mm/s, $\Delta E_Q$=0.66(1) mm/s, $\Gamma$=0.79(1) mm/s) and LS (S=1/2) Fe(III) ($\delta$=0.13(1) mm/s, $\Delta E_Q$=2.58(1) mm/s, $\Gamma$=0.37(1) mm/s), which are typical for Fe(III) $N_4O_2$ complexes at room temperature.[40] The area intensity ratio of HS Fe(III) to LS Fe(III) was found to be *ca.* 73%:27%, in agreement with the magnetization and X-ray data (see above).

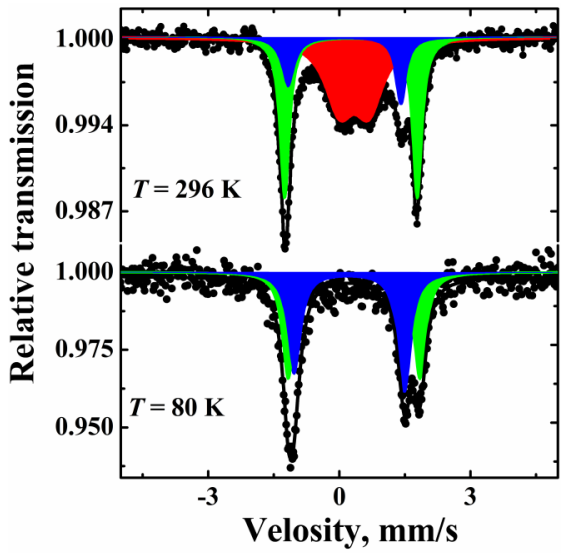


**Figure 6.** Mössbauer spectra for the [Fe(3-OMe-Sal$_2$trien)][Fe(tdas)$_2$]·$CH_3CN$ salt at 80 K and 296 K. Colored areas show the decomposition of the spectrum into components: green area corresponds to the contribution of [Fe(tdas)$_2$]$^-$ anion (S=3/2), blue area corresponds to the contribution of [Fe(3-OMe-Sal$_2$trien)]$^+$ cation in LS state (S=1/2) and red area corresponds to the contribution of SCO cation in HS state (S=5/2).

As deduced from the $\chi_M T$ value and X-ray analysis at 297 K, the ratio of HS:LS states in salt **1** is 75%:25% and 72%:28%, respectively. This perfect coincidence of $\gamma_{HS}$ values means that difference in HS/LS Lamb-Mössbauer factors for SCO cation is marginal at 296 K.[41] Since the HS and LS signals are distinct, we may infer that the spin state interconversion rate is still slow relative to the Mössbauer timescale.[42] The third doublet has Mössbauer parameters characteristic of [Fe(tdas)$_2$]$^-$ in intermediate spin state ($\delta$=0.28(1) mm/s, $\Delta E_Q$=3.03(1) mm/s, $\Gamma$=0.26(1) mm/s)[26] and represents *ca.* 38% of the iron ions in the sample. So the different Mössbauer intensities of [Fe(3-OMe-Sal$_2$trien)]$^+$ cation and [Fe(tdas)$_2$]$^-$ anion have to be attributed to different Lamb-Mössbauer factors.[43] One can conclude from the above data that dimeric [Fe(tdas)$_2$]$_2^{2-}$ anion does not demonstrate spin-crossover behavior and saves IS states on the Fe(III) centers. The valence of irons in **1** was confirmed to be Fe(III) for the [Fe(3-OMe-Sal$_2$trien)]$^+$ cation and the [Fe(tdas)$_2$]$^-$ anion.

## Theoretical calculations

### *DFT calculations of [Fe(3OMe-Sal$_2$-trien)]$^+$ conformers*

In earlier endeavor we reported on the relationship between iron(III) spin state and ethylene groups orientation in the [Fe(H$_2$-Sal$_2$-trien)]$^+$ spin-crossover complexes.[22] The ligand conformation can be determined by considering three five-membered rings: $FeN_2(CH_2)_2$. In each cycle the ethylene group (–C$^1$H$_2$–C$^2$H$_2$–) has two possible orientations: C$^1$ above C$^2$ relative to the plane of N–Fe–N (δ) or C$^1$ below C$^2$ (λ). The numbering of carbon atoms in the cycle is determined by counter-clockwise motion starting from the iron atom. Thus, the conformation of [Fe(Sal$_2$-trien)]$^+$ is uniquely determined by indicating the orientations of all three cycles. Besides, we proposed to classify the conformers in three types: **I** (all three cycles have the same orientation), **II** (the orientation of the middle cycle Fe(N$_{am}$)$_2$(CH$_2$)$_2$ differs from the orientation of the side cycles) and **III** (the orientation of the side cycle differs from the orientations of two remaining cycles). This classification indicates the symmetry of saltrien cation: $C_2$ for classes **I**, **II** and $C_1$ for class **III**. Moreover, it reflects the distribution of [Fe(Sal$_2$trien)]$^+$ conformers in the CCDC database.[22] It should be noted that [Fe(Sal$_2$trien)]-type complexes are chiral molecules, so we propose to consider only Δ-form of cation in this work. While for Λ-form the equivalent conformers will have opposite orientations of all cycles.

The SCO [Fe(3-OMe-Sal$_2$trien)]$^+$ cation in the structure [Fe(3-OMe-Sal$_2$trien)][Fe(tdas)$_2$]·$CH_3CN$ is presented by two conformers: Δ(λδλ) at 150K in LS state, Δ(λλλ) at 350K in HS state. It should be noted that the transition between the Δ(λδλ) (LS) and Δ(λλλ) (HS) conformers is the most common in the CCDC database.[22] The iron(III)-ligand bond lengths of conformers optimized structures are in a good agreement with experimental X-ray data (Table S5, Figure S14 in SI). Slight deviations in the values of the characteristic angle α are related to crystalline packing features.[27] The calculations demonstrate the energetic benefit for Δ(λδλ) conformer in LS state (8.6 kJ/mol) and for Δ(λλλ) conformer in HS state (9.5 kJ/mol) (Table 3). We also considered the electronic structures of conformers in both spin state in order to find out the reasons for the existence of Δ(λδλ) (LS)↔Δ(λλλ) (HS) transition. For all conformers, the global *Z* axis was chosen along the N$_{im}$-Fe-N$_{im}$ bond, whereas the *X*/*Y* axes were approximately aligned along N$_{am}$-Fe-O bonds. This facilitated identifying molecular orbitals of predominantly iron d orbital character.[44, 45] The orbital analysis was straightforward for MOs containing predominant contribution of iron e$_g$-like orbitals. Whereas the mixing of the MOs containing a predominant contribution of iron t$_{2g}$-like orbitals is much stronger in both spin states. This mixing apparently increases the degree of overlap between metal orbitals and π-donor ligand orbitals.[46]

**Table 3.** Electronic energies ($E_{el}$), zero-point vibration ($E_{ZPV}$) energies, total energies ($E_0$=$E_{el}$ + $E_{ZPV}$) and relative energies ($E_{rel}$) of the optimized [Fe(3-OMe-Sal$_2$trien)]$^+$ conformers in HS (S=5/2) and LS (S=1/2) states. These values were obtained from DFT calculations carried out at the B3LYP/6-311++G(d,p) level.

| Parameter | Conformer | | | |
|---|---|---|---|---|
| | Δ(λλλ) | | Δ(λδλ) | |
| | HS | LS | HS | LS |
| $E_{el}$, a.u. | -2639.0721282 | -2639.0692968 | -2639.0685497 | -2639.0724909 |
| $E_{ZPV}$, a.u. | 0.486902 | 0.490689 | 0.486926 | 0.490590 |
| $E_0$, a.u. | -2638.5852262 | -2638.5786078 | -2638.5816237 | -2638.5819009 |
| $E_{rel}$, kJ/mol | 0 | 8.64 | 9.46 | 0 |

The coordinates of optimized geometries are shown in Tables S17-S20.

The Δ(λδλ) conformer is realized only through LS state since the degree of σ-bonding in Δ(λδλ) conformer is stronger than that in Δ(λλλ) conformer, that increases the ligand-field splitting energy. Therefore Δ(λδλ) conformer is much more stable in LS state (Figure 7). MOs with predominant contribution of iron $d_{z^2}$ and $d_{x^2-y^2}$ orbitals for Δ(λδλ) conformer are destabilized by 0.111 eV and 0.105 eV relative to Δ(λλλ) conformer, respectively (Tables S6 and S7 in SI). Among iron $t_{2g}$-like orbitals of two conformers, MOs containing $d_{xy}$ orbitals are more destabilized that indicates a greater degree of iron/phenoxide π-bonding. Natural atomic charges also confirm the greater degree of π-bonding in Δ(λδλ) (LS) conformer: the minimum (positive) natural charge on Fe and the maximum (negative) natural charge on O (Table S8 in SI).[47]

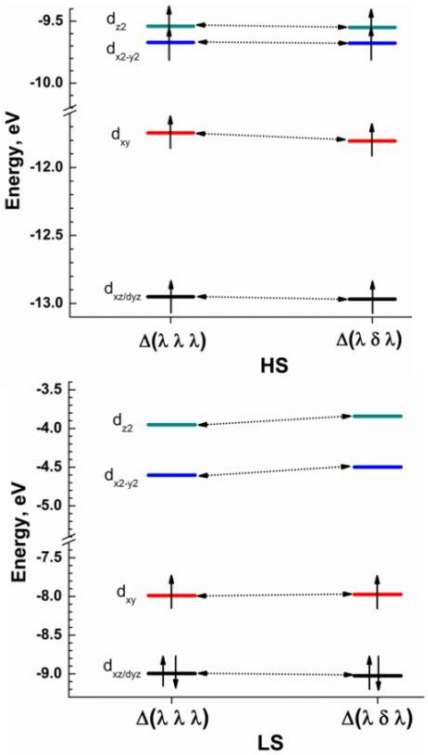


**Figure 7.** Energy levels diagram of molecular orbitals (B3LYP/6-311++G(d,p)) with predominant iron d orbitals contribution for HS (top) and LS (bottom) states of $[Fe(3\text{-}OMe\text{-}Sal_2trien)]^+$ conformers. For the LS system, the average energy of the relevant α and β spin MOs was used.

The calculated spin density distribution in the low- and high-spin conformers is shown in Figures S15 and S16, respectively. As seen, most of the spin density is concentrated at the iron(III) atom. The shape of spin density located in LS metal centers in Δ(λλλ) and Δ(λδλ) evidence that the unpaired electron resides in $d_{xy}$ orbital which is consistent with MO analysis (Figure 7 and S15 in SI).

In case of HS state, the Δ(λλλ) conformer is realized since the degree of π-bonding of phenoxide groups in Δ(λλλ) conformer is stronger than that in Δ(λδλ) conformer, that decreases the ligand-field splitting energy. Therefore Δ(λλλ) conformer is much more stable in HS state (Figure 7). MO containing predominant contribution of $d_{xy}$ orbital for Δ(λλλ) conformer is destabilized by 0.059 eV relative to Δ(λδλ) conformer. Furthermore, the MO with predominant contribution of iron $d_{xz/yz}$ orbitals is only slightly destabilized by 0.018 eV relative to Δ(λδλ) conformer (Tables S9 and S10 in SI). In the same way, natural atomic charges on Fe and O atoms confirm the greater degree of π-bonding in Δ(λλλ) (HS) conformer (Table S11 in SI).[47] It is also noteworthy that MO with a predominant contribution of iron $d_{z^2}$ and $d_{x^2-y^2}$ orbitals for Δ(λλλ) conformer are destabilized by 0.01 eV and 0.006 eV relative to Δ(λδλ) conformer, respectively. This means that a slightly greater degree of σ-bonding realizes in Δ(λλλ) (HS) conformer. Thus, the greater σ-/π-bonding for Δ(λλλ) HS and Δ(λδλ) (LS) conformers can apparently stabilize the saltrien-complex.

### *Exchange Coupling Constants from Broken-Symmetry DFT*

A broken-symmetry (BS) method is currently widely used because it captures the essential physics of spin-coupled systems and provides a practical approach to estimations of trends in experimental coupling constants.[48, 49] We used the BS method to evaluate the coupling constants (*J*) between the two paramagnetic centers in the dimeric $[Fe(tdas)_2]_2^{2-}$ anion. The calculations results were compared to the experimental data deduced from the *dc* magnetization measurements.

To obtain BS state for spin-zero complexes, the HS state was initially optimized and after that the spins on metal atoms were flipped for generating an antiferromagnetically coupled state. The resulting electronic structures were employed as a starting guess for geometry optimization of the BS states. For the system of two magnetic centers, the isotropic Heisenberg spin Hamiltonian is

$$\widehat{H} = -2J_{AB}\widehat{S_A}\cdot\widehat{S_B},$$

where $J_{AB}$ is the magnetic coupling between the unpaired electrons in sites A and B.

The *J* values were determined by following equations:

$$J = -\frac{E_{HS}-E_{BS}}{4S_AS_B} \qquad \text{Eq. } \mathbf{5}$$

$$J = -\frac{E_{HS}-E_{BS}}{4S_AS_B+2S_B} \qquad \text{Eq. } \mathbf{6}$$

$$J = -\frac{E_{HS}-E_{BS}}{<S^2_{HS}>-<S^2_{BS}>} \qquad \text{Eq. } \mathbf{7}$$

Where $E_{HS}$ and $E_{BS}$ denote computed energies in the HS ($S_{HS}=S_A+S_B$) and BS ($S_{BS}=S_A-S_B$) states; $S_A$ and $S_B$ are local spins of magnetic centers; $<S^2_{HS}>$ and $<S^2_{BS}>$ are total spin angular momentum of HS and BS states. Noodleman's spin-projected approach[50] (Eq. **5**) is considered to be valid in the "weak bonding" regime, while the alternative non-spin projected formula proposed by Ruiz and coworkers[51] (Eq. **6**) is derived in the strong overlap limit. In addition, the use of Yamaguchi formula[52] (Eq. **7**) covers the whole range of situations from the weak to the strong exchange coupling limit. The appropriateness of each approximation within DFT framework is still an open question in the literature.[53]

Ten functionals were employed in the present DFT-BS calculations of $J_2$ value for dimeric $[Fe(tdas)_2]_2^{2-}$ anion (Tables 4 and S12 in SI) since the accuracy of approximation strongly depends on the functional type. It is also worth noting that the exact Hartree-Fock (HF) exchange has a significant influence on the quantitative value of the exchange coupling constant.[54, 55]

**Table 4.** The values of $J_2$ calculated by formulas [Eq.(**5-7**)] and various density functionals for dimeric $[Fe(tdas)_2]_2^{2-}$ anion. The calculations were performed using 6-311++G(d,p) basis set.

| no. | DFT functional | Type | HF, % | $J_2(calc)$[a], K | | | $J_2(exp)$[b], K |
|---|---|---|---|---|---|---|---|
| | | | | Noodleman[50] | Ruiz[51] | Yamaguchi[52] | |
| 1 | PBE0[56] | GH-GGA | 25 | -63.3 | -47.5 | -63.2 | ***-99.47±0.19*** |
| 2 | B3LYP[57] | | 20 | -64.2 | -48.1 | -63.9 | |
| 3 | B3LYP*[58] | | 15 | -82.5 | -61.8 | -82.0 | |
| 4 | O3LYP[59] | | 11.61 | -68.6 | -51.4 | -68.3 | |
| 5 | B3LYP**[60] | | 10 | -108.1 | -81.1 | -107.2 | |
| 6 | MPWLYP1M[61] | | 5 | -118.2 | -88.7 | -116.8 | |
| 7 | TPSSh[62] | GH-mGGA | 10 | ***-102.5*** | -76.9 | ***-101.7*** | |
| 8 | TPSS[63] | mGGA | | -175.2 | -131.4 | -171.6 | |
| 9 | OLYP[64] | GGA | – | -111.4 | -83.5 | -110.1 | |
| 10 | BLYP[65] | | | -148.2 | -111.2 | -145.4 | |

[a] The total energies ($E_0$(HS/BS) = $E_{el}$ + $E_{ZPV}$) were applied for calculations by Equations (**5-7**). In the case of dimeric $[Fe(tdas)_2]_2^{2-}$ anion: $S_A(Fe)=S_B(Fe)=3/2$. Reasonable agreement of calculated and experimental values of $J_2$ selected bold italics.

[b] The value corresponds to the experimental structure of **1**.

The coordinates of optimized geometries are shown in Tables S21-S26 and S29-S32 in SI.

The calculated $J_2$ values for dimeric $[Fe(tdas)_2]_2^{2-}$ anion are indicated in Table 4, all functionals correspond to antiferromagnetic interactions. Noodleman and Yamaguchi equations give almost identical values; the difference is less than ~2%. For Ruiz equation, the exchange coupling constant values are underestimated by ~25% respect to values obtained from the Noodleman and Yamaguchi equations.

Obtained results reveal a strong dependence on exact HF exchange indeed, data show a general decrease in the $J_2(calc)$ values with increasing of HF exchange. At the same time, GGA and mGGA functionals overestimate the strength of AFM coupling. The closest to experimental value of $J_2$ is calculated using the TPSSh functional by Noodleman and Yamaguchi equations. There are many of examples that hybrid functionals better describe the nature of antiferromagnetic bond comparing to pure functionals but hybrid functionals tend to give a poorer geometry of complex including unduly long metal–ligand bonds.[49, 66]

Therefore, it is of interest to compare the parameters of the optimized structures of $[Fe(tdas)_2]_2^{2-}$ complex with X-ray data (Figure S17 and Table S13 in SI). In this respect it should be noted that the calculated interlayer distance (*Fe(1)-S(18)/Fe(16)-S(3),* Figure S17 in SI) in the $[Fe(tdas)_2]_2^{2-}$ are slightly overestimated by all functionals. Nonetheless, the TPSS and TPSSh functionals demonstrate the closest to experimental value of interlayer distance. The selected φ (*Fe(1)-S(18)-Fe(16)/Fe(1)-S(3)-Fe(16),* Figure S17 in SI) angle is greater than 90˚ for all functionals, except for TPSS, TPSSh and PBE0, while φ angle is less than 90˚ for experimental structures. Then it turns out that the TPSSh functional demonstrates excellent correlation between experimental and calculated data both in the exchange coupling parameter $J_2(exp)$ and structure. The difference between calculated and experimental bond lengths in TPSSh-optimized structure of $[Fe(tdas)_2]_2^{2-}$ does not exceed 0.03 Å. To study the influence of small geometric modifications on the calculated exchange coupling constant, we also calculated the $J_2$ values using TPSSh functional for the fixed geometry of dimeric $[Fe(tdas)_2]_2^{2-}$ anion, obtained from the X-ray data at 150K, 297K and 350K (Table S14 in SI). These calculations show that $J_2(calc)$ values in absolute magnitude are almost two times higher than the reported experimental values. In the present case geometry optimization of $[Fe(tdas)_2]_2^{2-}$ leads to a significant decline in the energies of the HS and BS states, which affects the ΔE(HS-LS)=$E_{el}$(HS) - $E_{el}$(BS) value.

In addition to the magnetic exchange constant, it is important to study the spin density (SD) distribution in the $[Fe(tdas)_2]_2^{2-}$ spin dimer. To understand the exchange pathway, the Mulliken population analysis for dimeric anion was performed using the TPSSh functional for HS (S=3) state and BS (S=0) state, where positive and negative signs denote α and β spin states, respectively (Table S15 in SI). The SD plots of $[Fe(tdas)_2]_2^{2-}$ are shown in Figure 8.

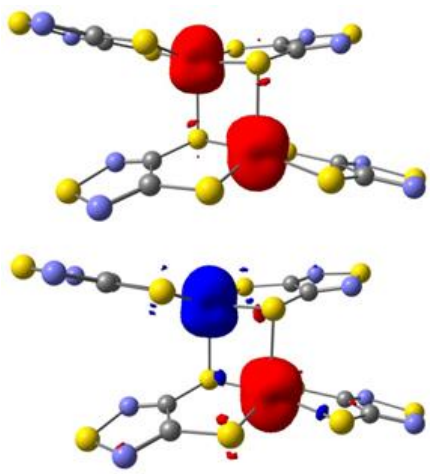

**Figure 8.** Spin density plots of dimeric $[Fe(tdas)_2]_2^{2-}$ anion corresponding to HS (top) and BS (bottom) states: red, positive spin density; blue, negative spin density. The isodensity surfaces are plotted with the cut-off values of 0.0095 $eÅ^{-3}$ for HS state and 0.008 $eÅ^{-3}$ for BS state. TPSSh functional was used.

In both states, the predominant SD is located on the iron atoms of dimer with only minor delocalization over the nearest donor atoms of the $tdas^{2-}$ ligands. The SDes on the two iron centers in BS sate have the same absolute values but opposite signs (Figure S17 and Table S15 in SI): Fe(1) atom has unpaired electrons with α(↑) spin and Fe(16) atom has unpaired electrons with β(↓) spin.

In the case of HS sate, the SDes on sulfur atoms S(3) and S(18) located near Fe(1) and Fe(16) atoms, respectively, are equal to ρ=0.083 *e*, whereas the SDes on sulfur atoms S(3) ρ=-0.042 *e* and S(18) ρ=0.042 *e* are decreased twice for BS sate. The decrease of the spin population on the sulfur atoms S(3) and S(18) can be associated with the delocalizing effect from the two iron centers. It also displays that the sulfur S(3) atom is mainly influenced by the delocalization from Fe(16) neighboring atom, while for the sulfur S(18) atom, the delocalization from Fe(1) neighbor atom is predominant. Obviously, in this binuclear structure the effect of the spin delocalization results in antiferromagnetic interaction.[67]

It is also of interest to estimate the possibility of a SCO phenomenon in the $[Fe(tdas)_2]_2^{2-}$ dimer. Since the "reentrant" behavior in magnetic properties of ($n$Bu$_4$N)[Fe(tdas)$_2$] salt was detected by K. Awaga *et al*.,[24] MPWLYP1M functional was used for this estimation because it demonstrated good accuracy in reproducing the experimental data of exchange coupling constants in ($n$Bu$_4$N)[Fe(tdas)$_2$]: $J_2/k_B(exp)$=-118 K,[24] $J_2(calc)$= -118.2 K (Noodleman's approach, Table 4). According to calculated energy distribution of $[Fe(tdas)_2]_2^{2-}$ dimer with possible iron spins: $S_A$=$S_B$=1/2, 3/2 and 5/2, the structure with antiferromagnetic interactions of iron centers with $S_A$=$S_B$=3/2 is more energetically favorable, which is completely consistent with the above experimental data (Figures S18, S19, Table S16 in SI). The existence of AFM exchange coupling in the dimer with $S_A$=$S_B$=3/2 is energetically beneficial by 8.85 kJ/mol compared to analogous HS Fe(α,↑)-Fe(α,↑) structure. The dimeric structures with $S_A$=$S_B$=1/2 and 5/2 spins are not energy minima in the cases of HS and BS states (>80 kJ/mol). Received result allows us to completely eliminate the possibility of SCO behavior, because the main criterion for the appearance of SCO is the energy proximity of two spin states. Thus, this confirms the earlier conclusion[26] based on $^{57}$Fe Mössbauer spectroscopy study of ($n$Bu$_4$N)[Fe(tdas)$_2$] salt: the "reentrant" phase transition can be associated only with the decrease of exchange coupling constant in the dimer.

## Conclusion

A joint experimental and theoretical study has allowed to highlight the properties of the novel salt [Fe(3-OMe-Sal$_2$trien)][Fe(tdas)$_2$]·CH$_3$CN (**1**) showing multimagnetic properties. This salt has been thoroughly characterized by single crystal X-ray diffraction methods at 150, 297 and 350 K which show that the crystal structure consists of alternating layers composed by parallel arrangements of the chains of isolated π-π coupled pairs of cations and dimerized $[Fe(tdas)_2]^-$ anions. The magnetic behavior of **1** has shown that the *dc* magnetic susceptibility is determined by the sum of the contributions from cations showing spin-crossover behavior and strong AFM coupled dimeric $[Fe(tdas)_2]_2^{2-}$ anions. The $[Fe(3\text{-}OMe\text{-}Sal_2trien)]^+$ cation exhibits gradual SCO transition ($T_{1/2}$=195 K) with a weak cooperativity effect and a narrow thermal hysteresis of 6 K. The *dc* magnetization and $^{57}$Fe Mössbauer spectroscopy measurements at room temperature give excellent agreement between $\gamma_{HS}$(%) value and the ratio of disordering of ethylene groups determined from X-ray analysis. Nevertheless, ethylene groups disordering is strongly dependent on cooperative effects and features of crystal packing. The experimental $J_2$ value is in agreement with the calculated one and also with magneto-structural data of previously synthesized compound containing $[Fe(tdas)_2]_2^{2-}$ anion. DFT calculations suggest also that ethylene groups rearrangement in the cation determines the stabilization of the spin state. This finding provides a qualitative estimate of the content of the HS fraction from X-ray structural data.

The synthesis, the full characterization as well as theoretical studies of [Fe(3-OMe-Sal$_2$trien)][Fe(tdas)$_2$]·CH$_3$CN, represent an important achievement addressed to optimize the molecular design of new multifunctional materials based on salts of SCO cation and dimerized anion pairs. The communication between ions through intermolecular interactions, which could control the molecular arrangement and the spin state to afford well-ordered crystal structures was clarified for understanding the involved microscopic mechanisms, which are of fundamental importance for practical applications.

## Experimental Section

***Electron-probe X-ray microanalysis (EPMA).*** *EPMA* was performed with a Zeiss Supra-25 analytical field emission electron microscope equipped with a Gemini electron optical column at magnification varying from 600 to 6200 depending on the sample and the electron beam energy of 9.7-20 keV. The depth of beam penetration into the sample was 1-3 μm.

***Powder X-Ray Diffraction (PXRD).*** *PXRD* was measured using a Siemens D500 powder diffractometer with linear detector at room temperature (CuKα1 - radiation, λ = 1.5406 Å, step = 0.02°, single crystal cuvette). Powder patterns were used as a fingerprint for identification of the crystalline phase presented in a material.

***Thermogravimetric Analysis.*** The thermogravimetric analysis was performed in argon atmosphere at a heating rate of 5 °C min$^{-1}$ using a *NETZSCH STA 409 C Luxx* thermal analyzer, which allows simultaneous measurements of thermogravimetry (*TG*) and differential scanning calorimetry (*DSC*). Mass of sample 8.33 mg, temperature range 30 – 350 °C.

***IR spectroscopy.*** The FTIR absorbance spectra were recorded at room temperature in the range 400–4000 cm$^{-1}$ (50 scans, resolution 4 cm$^{-1}$) using FTIR Bruker model Vertex 70V spectrometer (Germany). The attenuated total reflectance (ATR) method of registration (ATRM) was performed using Platinum-ATR (Bruker) accessory equipped with a diamond crystal, without preliminary sample preparation.

***Single-crystal structure determinations.*** Single crystal X-ray diffraction experiments were carried out on an Oxford Diffraction GeminiR CCD diffractometer (λ(MoKα) = 0.71073 Å, graphite monochromator, ω-scan mode) at 150K, 297K and 350K. Data reduction and empirical absorption correction of experimental intensities (SCALE3ABSPACK) were made by the CrysAlisPro program.[68] The structure was solved by charge flipping method using Superflip program[69] and refined by the full-matrix least-squares technique against $F^2$ in an anisotropic approximation for all non-hydrogen atoms using SHELXL program.[70] Hydrogen atoms were placed according to geometry and residual electron density peaks. Selected crystallographic data and refinement parameters are given in SI Table S4. A CCDC numbers 1996141-1996143.

***Magnetic measurements.*** Magnetic properties of [Fe(3-OMe-Sal$_2$trien)][Fe(tdas)$_2$]·CH$_3$CN were investigated using the VSM option of "Quantum Design" Physical Properties Measurements System PPMS – 9T on the fine powder sample with mass of about 5 mg placed into the plastic capsule. The temperature dependence of *dc* magnetic

susceptibility $\chi$ has been taken at warming and cooling modes (temperature range of 2–350 K) in a magnetic field *B*=0.1 T. The molar magnetic susceptibility was corrected to diamagnetic contribution calculated as a sum of Pascal constants ($-9\cdot10^{-5}$ $cm^3\cdot mol^{-1}$).[71] The temperature dependence of the magnetic susceptibility ($\chi$) of **1** was performed on finely ground microcrystalline powders.

***$^{57}$Fe Mössbauer spectroscopy.*** $^{57}$Fe Mössbauer absorption spectra of complexes **1**-**3** were recorded on a WissEl (Germany) spectrometer operating in a constant acceleration mode. $^{57}$Co in the Rh matrix was used as the source. Spectra at low temperatures were measured using a continuous flow helium cryostat CF-506 (Oxford Instruments) with controllable temperature. Mossbauer absorption spectra were processed by the least square method assuming the Lorentzian shape of the individual spectral components. Isomer shift values were taken with respect to iron metal.

***Computation details.*** All density functional theory (DFT) calculations were carried out using the Gaussian 09 computational package[72] on an servers and workstations of the Institute of Problems of Chemical Physics Russian Academy of Sciences, Chernogolovka. Calculations of the iron(III) complexes were performed with an unrestricted wave function. Geometry optimizations were done without any symmetry constrains. Molecular geometries and orbitals (MOs), electronic energies ($E_{el}$) and vibrational frequencies were calculated using the Pople's group split-valence 6-311++G(d,p) basis set.[73] Zero point vibration energies ($E_{ZPV}$) for the total energy $E_0$ ($E_0 = E_{el} + E_{ZPV}$) were obtained by the harmonic oscillator approximation. The energy minima for all optimized structures were verified by vibration frequency calculations: imaginary frequencies were not found. Natural atomic charges were obtained using the NBO 3.1 module[74] in Gaussian 09. The atomic coordinates for starting geometries of $[Fe(3\text{-}OMe\text{-}Sal_2trien)]^+$ and $[Fe(tdas)_2]_2^{2-}$ were taken from the X-ray crystallographic data (this work). Calculations for $[Fe(3\text{-}OMe\text{-}Sal_2trien)]^+$ conformers were performed using the hybrid B3LYP functional. Exchange interaction parameter was evaluated within broken symmetry approximation (DFT-BS) by Ginsberg, Noodleman, Yamaguchi and others.[75, 76, 77] Ten functionals were used in calculations of dimeric anion $[Fe(tdas)_2]_2^{2-}$ for both the high spin (HS) and broken-symmetry (BS) spin-states. Negative value for *J* corresponds to antiferromagnetic interaction.

***Synthesis***

Commercial solvents were used without further purification unless otherwise specified. Reactants commercially obtained: 3-methoxysalicylaldehyde, 1,8-diamino-3,6,-diazaoctane, iron nitrate nonahydrate $[Fe(NO_3)_3\cdot 9H_2O]$ and sodium methoxide ($CH_3ONa$) from Sigma-Aldrich (Saint Louis, MO, USA).
Complexes ($n$Bu$_4$N)[Fe(tdas)$_2$] (**2**) and $[Fe(3\text{-}OMe\text{-}Sal_2trien)]NO_3\cdot H_2O$ (**3**) were prepared according to the general methods described previously in literature.[23b ,30]
The purity of the complexes and their solvation state were verified by determining the carbon, hydrogen, nitrogen and sulfur content, at the Vario MICRO Cube Elementar GmbH Analysis Service.

**($n$Bu$_4$N)[Fe(tdas)$_2$]** (**2**) (tdas - 1,2,5-thiadiazole-3,4-dithiolate)
Complex **2** was prepared according to the general methods described previously. Elemental Anal. Found: C, 40.10; H, 5.93; N, 11.51; S 22.13 %. Calcd for ($M_w$= 594 $g\cdot mol^{-1}$ ) $C_{20}H_{36}N_5S_6Fe$: C, 40.40; H, 6.10; N, 11.78; S, 22.22; Fe, 9,43%.

**$[Fe(3\text{-}OMe\text{-}Sal_2trien)]NO_3\cdot H_2O$** (**3**). (3-OMe-Sal$_2$trien=N,N'-bis[2-(2-hydroxy-3-methoxysalicylaldehyde)ethyl]ethane-1,2-diamine).
Condensation of the 3-methoxysalicylaldehyde with triethylenetetramine and subsequent metalation with iron(III) nitrate, *in situ* afforded the complex **3.** The crude solid was recrystallised from warm water to give dark violet microcrystals, which were collected and dried *in vacuo* over $P_2O_5$. Elemental Anal. Found: C, 47.73; H, 5.25; N, 12.74; Fe, 10.43%. Calcd for ($M_w$ = 548.36 $g\cdot mol^{-1}$) $C_{22}H_{30}FeN_5O_8$: C, 48.18; H, 5.47; N, 12.77; Fe, 10.21%.

**$[Fe(3\text{-}OMe\text{-}Sal_2trien)][Fe(tdas)_2]\cdot CH_3CN$** (**1**). The synthesis of **1** is very straightforward and facile: to the stirred solution of (n-Bu$_4$N)[Fe(tdas)$_2$] (84 mg, 0.15 mmol) in acetonitrile ($CH_3CN$, 15 mL) was added dropwise a solution of $[Fe(3\text{-}OMe\text{-}Sal_2trien)]NO_3\cdot H_2O$ (82 mg, 0.15 mmol) in $CH_3CN$ (10 mL). The reaction mixture was further stirred under heating for 10 min, then filtered off through the paper filter and cooled in refrigerator. The precipitate appeared after 2 days was filtered from mother liquor, washed with cooled acetonitrile, and dried *in vacuo* over $P_2O_5$ at room temperature. $[Fe(3\text{-}OMe\text{-}Sal_2trien)][Fe(tdas)_2]\cdot CH_3CN$ (**1**) was obtained as black polycrystalline powder with a total yield 88.14%. Elemental Anal. Found: C, 39.00; H, 3.58; N, 14.57; S, 22.30; Fe, 12.32%. Calcd for (Mw = 861.68 $g\cdot mol^{-1}$) $C_{28}H_{31}Fe_2N_9O_4S_6$: C, 39.02; H, 3.60; N, 14.63; S, 22.28; Fe, 12.99%.
By means of slow diffusion method in U-shaped cell solution of ($n$Bu$_4$N)[Fe(tdas)$_2$] (6 mg, 0.01 mmol) in acetone (4 mL) diffused into solution of $[Fe(3\text{-}OMe\text{-}Sal_2trien)]NO_3\cdot H_2O$ (5.5 mg, 0.01 mmol) in acetonitrile (1 mL), after one week the shine black crystals of **1** suitable for X-ray diffraction were filtered and dried at ambient temperature.

## Acknowledgements

We acknowledge funding from the Ministry of Science and Higher Education of the Russian Federation (Grant No. 075-15-2020-779; A.V. and O.M. by contracts 02.A03.21.0004, 02.A03.21.0011).This work was partially done on the topic of the State task, state registration No AAAA-A19-119092390079-8, AAAA-A19-119032690060-9 with using of the Computational and Analytical Center for Collective Use of the IPCP and ISSP RAS tool base. Partially the study was carried out within the state assignment for the ISSP RAS. O.M. acknowledges support by NUST "MISiS", grant K2-2020-008. P.D. and L.P. acknowledge Università degli Studi di Cagliari for supporting this research.

**Conflicts of Interest:** The authors declare no conflict of interest. The founding sponsors had no role in the design of the study; in the collection, analyses, or interpretation of data; in the writing of the manuscript, and in the decision to publish the results.

**Keywords:** spin-crossover • iron(III) complexes • multi-magnetic salt • saltrien-type • 1,2,5-thiadiazole-3,4-dithiolate

[1] a) J. Olguín, Coord. *Chem. Rev.* **2020**, *407*, 213148-213177. b) A. Bousseksou, G Molnár, L. Salmona, W. Nicolazzi, *Chem. Soc. Rev*. **2011**, *40*, 3313-3335.
[2] A. Tissot, X. Kesse, S. Giannopoulou, I. Stenger, L. Binet, E. Rivière, C. Serre, *Chem. Commun.* **2019**, *55*, 194-197.
[3] T. Kitazawa, *Crystals.* **2019**, 9, 8, 382.
[4] I. Nemec, P. Zoufalý, P. Jewula, P. Antal, W. Linert, R. Herchel, *New J. Chem*. **2019**, *43*, 4937-4946.
[5] G. Molnár, S. Rat, L. Salmon, W. Nicolazzi, A. Bousseksou, *Adv. Mater*. **2018**, *30*, 1–23.
[6] H. Li, H. Peng, *Current Opinion in Colloid & Interface Science***.** **2018**, *35*, 9–16.
[7] K. S. Kumar, M. Ruben, *Coord. Chem. Rev*. **2017**, *346*, 176-205.
[8] J. Dugay, M. Aarts, M. Giménez-Marqués, T. Kozlova, H. W. Zandbergen, E. Coronado, H. S. J. van der Zant, *Nano Lett.* **2017**, *17*, 1, 186-193.
[9] J.F. Létard, P. Guionneau, L. Goux-Capes, *Top. Curr. Chem*. **2004**, *235*, 221-249.

[10] M. Nihei, T. Shiga, Y. Maeda, H. Oshio, *Coord. Chem. Rev*. **2007**, 251, 2606-2621.

[11] P. Gütlich, H.A. Goodwin, *Top. Curr. Chem*. **2004**, 233, 1-47.

[12] a) O. Sato, Z.-Y. Li, Z.-S. Yao, S. Kang, S. Kanegawa, in Spin-Crossover Materials: Properties and Applications, (Ed. M. A. Halcrow), A John Wiley & Sons, Ltd, Chichester, **2013,** *11*, 303–319. (b) P. Deplano, L. Leoni, M. L. Mercuri, J. A. Schlueter, U. Geiser, H. H. Wang, A. M. Kini, J. L. Manson, C. J. Gómez-García, E. Coronado, H.-J. Koo, M.-H. Whangbo, *J. Mater. Chem.*, **2002**, *12*, 3570-3577. c) L. Pilia, C. Faulmann, I. Malfant, V. Collière, M. L. Mercuri, P. Deplano, P. Cassoux, *Acta Crystallogr. Sec. C.* **2002**, 58, 4, 240-242. d) N. Robertson, K. Awaga, S. Parsons, A. Kobayashi, A. E. Underhill, *Adv. Mater. Opt. Electron.* **1998**, 8, 2, 93-96. e) A. E. Underhill, N. Robertson, J. Ziegenbalg, N. L. Narvor, J. D. Kilburn, K. Awaga, *Mol. Crysr. Liq. Cryst.* **1996**, *284*, 39-48.

[13] a) S. Dorbes, L. Valade, J. A. Real, C. Faulmann, *Chem. Commun*. **2005**, 69-71. b) C. Faulmann, S. Dorbes, J. A. Real L. Valade, *J. Low Temp. Physics*. **2006**, *142*, 265-270. c) L. C. J. Pereira, A. M. Gulamhussen, J. C. Dias, I. C. Santos M. Almeida, *Inorg. Chim. Acta*. **2007**, *360*, 3887-3895.

[14] M. Clemente-León, E. Coronado, M. López-Jordà, J. C. Waerenborgh, *Inorg. Chem*. **2011**, *50*, 18, 9122-9130.

[15] a) M. Clemente-León, E. Coronado, M. López-Jordà, C. Desplanches, S. Asthana, H. Wang, J.-F. Létard, *Chem. Sci.* **2011**, *2*, 1121-1127. b) M. Clemente-Leon, E. Coronado, C. Martí-Gastaldo, F. M. Romero, *Chem. Soc. Rev.,* **2011**, *40*, 473-497. c) M. Clemente-León, E. Coronado, M. López-Jordà, J. C. Waerenborgh, C. Desplanches, H. Wang, J.-F. Létard, A. Hauser, A. Tissot, *J. Am. Chem. Soc*. **2013**, *135*, 23, 8655-8667.

[16] C. Gandolfi, G. G. Morgan, M. Albrecht, *Dalton Trans*. **2012**, *41*, 3726-3730.

[17] C. Johnson, G. G. Morgan, M. Albrecht, *J. Mater. Chem. C*. **2015**, *3*, 7883-7889.

[18] P. N. Martinho, T. Lemma, B. Gildea, G. Picardi, H. Müller-Bunz, R. J. Forster, T. E. Keyes, G. Redmond, G. G. Morgan, *Angew. Chem*., **2012**, *51*, 11995-11999.

[19] C. Gandolfi, C. Moitzi, P. Schurtenberger, G. G. Morgan, M. Albrecht, *J. Am. Chem. Soc*. **2008**, *130*, 44, 14434-14435.

[20] H.-B. Duan, X.-R. Chen, H. Yang, X.-M. Ren, F. Xuan, S.-M. Zhou, *Inorg.Chem*., **2013**, *52*, 7, 3870-3877.

[21] N. G. Spitsyna, Y. N. Shvachko, D. V. Starichenko, E. Lahderanta, A. A. Komlev, L. V. Zorina, S. V. Simonov, M. A. Blagov, E. B. Yagubskii, *Crystals*. **2018**, *8*, 10, 382.

[22] M. A. Blagov, V. B. Krapivin, S. V. Simonov, N. G. Spitsyna, *Dalt. Trans*. **2018**, *47*, 16040-16043.

[23] a) S. Sproules, K. Wieghardt, *Coord. Chem. Rev*. **2010**, *254*, 1358-1382. b) I. Hawkin, A. E. Underhill. *J. Chem. Soc. Chem. Commun*. **1990**, 1593-1594.

[24] K. Awaga, T. Okuno,Y. Maruyama, A. Kobayashi, H. Kobayashi, S. Schenk, A. E. Underhill, *Inorg. Chem*. **1994**, *33*, 24, 5598-5600.

[25] S. Alvarez, R. Vicente, R. Hoffmann, *J. Am. Chem. Soc*. **1985**, *107*, 22, 6253-6277.

[26] M. Takahashi, M. Takeda, K. Awaga, T. Okuno,Y. Maruyama, A. Kobayashi, H. Kobayashi, S. Schenk, N. Robertson, A. E. Underbill, *Mol. Cryst. Liq. Cryst*. **1996**, *286*, 77-82.

[27] R. Pritchard, S. A. Barrett, C. A. Kilner, M. A. Halcrow, *Dalt. Trans*. **2008**, 3159-3168.

[28] M. A. Halcrow, *Crystals*. **2016**, *6*, 58.

[29] B. S. Lim, R. H. J. Holm, *Am. Chem. Soc.* **2001**, *123*, 1920–1930. (a) L. Canali, D. C. Sherrington. *Chem. Soc. Rev.* **1999**, *28*, 85–93.

[30] M. F. Tweedle, L. J. Wilson, *J. Am. Chem. Soc.* **1976**, *98*, 4824-4834.

[31] CCDC no. 1417015.

[32] a) P. Kuppusamy, P. T. Manoharan, *Proc. Indian Acad. Sci. (Chem. Sci.).* **1987**, *98*, 115-129. b) A. Ehnbom, S. K. Ghosh, K. G. Lewis, J. A. Gladysz, *Chem. Soc. Rev.,* **2016**, *45*, 6799-6811.

[33] A. H. Ewald, R. L. Martin, E. Sinn, A. H. White. *Inorg. Chem.***1969**, *8*, 9, 1837-1846.

[34] A. H. Ewald, R. L. Martin, I. G. Ross, A. H. White. *Proc. R. Soc. Lond. A*. **1964**, *280*, 235-257.

[35] M. Okai, K. Takahashi, T. Sakurai, H. Ohta, T. Yamamoto, Y. Einaga, *J. Mater. Chem. C*. **2015**, *3*, 7858-7864.

[36] I. Nemec, R. Herchel, I. Šalitroš, Z. Trávníček, J. Moncoľ, H. Fuess, M. Ruben, W. Linert, *CrystEngComm*. **2012**, *14*, 7015–7024.

[37] J. Huang, M. Kertesz. *J. Am. Chem. Soc.* **2007**, *129*, 1634-1643.

[38] Y. Maeda, H. Oshio, Y. Tanigawa, T. Oniki, Y. Takashima, *Bull. Chem. Soc. Jpn.* **1991**, *64*, 1522-1527.

[39] S. Singhal, C. L. Sharma, A. N. Garg, K. Chandra. *Transition Metal Chemistry*. **2001**, *26*, 81-88.

[40] Y. Maeda, Y. Takashima. *Comments Inorg. Chem.* **1988**, *7*, 1, 41-52.

[41] C. M. Grunert, H. A. Goodwin, C. Carbonera *et al*. *J. Phys. Chem. B.* **2007**, 111, 6738-6747.

[42] M. Clemente-León, E. Coronado, M. López-Jordà, J.-F. Létard, J. Kusz, P. Gütlich, *Chem. Eur. J.* **2010**, *16*, 2207-2219.

[43] L. Wiehl, *Acta Cryst.* **1993**. B49, 289-303.

[44] S. Amabilino, R. J. Deeth, *Inorg. Chem*. **2017**, *56*, 5, 2602-2613.

[45] G. Novitchi, S. Jiang, S. Shova, F. Rida, I. Hlavička, M. Orlita, W. Wernsdorfer, R. Hamze, C. Martins, N. Suaud, N. Guihéry, A.-L. Barra, C. Train, *Inorg. Chem*. **2017**, *56*, 24, 14809-14822.

[46] J. P. Holland, N. Vasdev, *Dalton Trans*. **2014**, *43*, 9872-9884.

[47] J. Conradie, *S. Afr. J. Chem.*, **2010**, 63, 65-71.

[48] Y. Kitagawa, T. Saito, K. Yamaguchi. DOI: 10.5772/intechopen.75726.

[49] K. H. Hopmann, L. Noodleman, A. Ghosh, *Chem. Eur. J.* **2010**, *16*, 10397-10408.

[50] L. Noodleman, *J. Chem. Phys.* **1981**, 74, 5737-5743.

[51] E. Ruiz, J. Cano, S. Alvarez, P. Alemany, *J. Comput. Chem. Vol.* **1999**, *20*, 13, 1391-1400.

[52] M. Mitani, H. Mori, Y. Takano, D. Yamaki, Y. Yoshioka, K. Yamaguchi, *J. Chem. Phys.* **2000**, *113*, 4035-4051.

[53] D. A. Pantazis, V. Krewald, M. Orio, F. Neese, *Dalton Trans.* **2010**, *39*, 4959-4967.

[54] N. A. G. Bandeira, B. L. Guennic, *J. Phys. Chem. A.* **2012**, *116*, 13, 3465-3473.

[55] M. Č. Romanović, B. R. Čobeljić, A. Pevec, I. Turel, V. Spasojević, A. A. Tsaturyan, I. N. Shcherbakov, K. K. Anđelković, M. Milenković, D. Radanović, M. R. Milenković, *Polyhedron*. **2017**, *128*, 30-37.

[56] C. Adamo, V. Barone, *J. Chem. Phys.* **1999**,*110*, 6158-69.

[57] A. D. Becke, *J. Chem. Phys.* **1993**, *98*, 5648-52.

[58] M. Reiher, *Inorg. Chem.* **2002**, *41*, 25, 6928-6935.

[59] A. J. Cohen, N. C. Handy, *Mol. Phys.* **2001**, *99*, 607-615.

[60] I. Respondek, L. Bressel, P. Saalfrank, H. Kämpf, A. Grohmann, *Chem. Phys.* **2008**, *347*, 514-522.

[61] N. E. Schultz, Y. Zhao, D. G. Truhlar, *J. Phys. Chem. A.* **2005**, *109*, 49, 11127-11143.

[62] N. Staroverov, G. E. Scuseria, J. Tao, J. P. Perdew, *J. Chem. Phys.* **2003**, 119, 12129-12137.

[63] J. Tao, J. P. Perdew, V. N. Staroverov, G. E. Scuseria, *Phys. Rev. Lett.* **2003**, 91, 146401.

[64] N. C. Handy, A. J. Cohen, *Mol. Phys.* **2001**, 99, 5, 403-412.

[65] A. D. Becke, *Phys. Rev. A*. **1988**, 38, 3098-3100.

[66] K. H. Hopmann, J. Conradie, A. Ghosh, *J. Phys. Chem. B.* **2009**, 113, 30, 10540-10547.

[67] Y. Sun, L. Wang, J. Wu, *Transition Met. Chem.* **2008**, 33, 1035-1040.

[68] O. D. Rigaku, CrysAlis PRO Software system version 1.171. 39.46. Rigaku Corporation, **2018**.

[69] L. Palatinus, G. Chapuis. *J. Appl. Cryst*. **2007**, *40*, 786-790.

[70] G.M. Sheldrick. *Acta Cryst*. **2008**, *A64*, 112-122.

[71] G.A. Bain, J.F. Berry, *J. Chem. Educ*. **2008**, *85*, 4, 532-536.

[72] M. J. Frisch, G. W. Trucks, H. B. Schlegel, G. E. Scuseria, M. A. Robb, J. R. Cheeseman, G. Scalmani, V. Barone, B. Mennucci, G. A. Petersson, H. Nakatsuji, M. Caricato, X. Li, H. P. Hratchian, A. F. Izmaylov, J. Bloino, G. Zheng, J. L. Sonnenberg, M. Hada, M. Ehara, K. Toyota, R. Fukuda, J. Hasegawa, M. Ishida, T. Nakajima, Y. Honda, O. Kitao, H. Nakai, T. Vreven, J. A. Montgomery, Jr., J. E. Peralta, F. Ogliaro, M. Bearpark, J. J. Heyd, E. Brothers, K. N. Kudin, V. N. Staroverov, T. Keith, R. Kobayashi, J. Normand, K. Raghavachari, A. Rendell, J. C. Burant, S. S. Iyengar, J. Tomasi, M. Cossi, N. Rega, J. M. Millam, M. Klene, J. E. Knox, J. B. Cross, V. Bakken, C. Adamo, J. Jaramillo, R. Gomperts, R. E. Stratmann, O. Yazyev, A. J. Austin, R.

Cammi, C. Pomelli, J. W. Ochterski, R. L. Martin, K. Morokuma, V. G. Zakrzewski, G. A. Voth, P. Salvador, J. J. Dannenberg, S. Dapprich, A. D. Daniels, O. Farkas, J. B. Foresman, J. V. Ortiz, J. Cioslowski, and D. J. Fox, Gaussian 09, Revision B.01, Gaussian, Inc., Wallingford CT, **2010**.

[73] J. A. Pople, M. Head-Gordon, K. Raghavachari, *J. Chem. Phys*., **1987**, 87, 5968.

[74] E. D. Glendening, J. K. Badenhoop, A. E. Reed, J. E. Carpenter, J. A. Bohmann, C. M. Morales, F. Weinhold, NBO 3.1, Theoretical Chemistry Institute, University of Wisconsin, Madison, WI, USA, **2001**.

[75] A.P. Ginsberg. *J. Am. Chem. Soc*. **1980**, *102*, 111-117.

[76] L. Noodleman, C. Y. Peng, D. A. Case, J. M. Mouesca. *Coord. Chem. Rev*. **1995**, *144*, 199-244.

[77] K. Yamaguchi, Y. Takahara, T. Fueno (Eds.: J.V.H. Smith, H.F. Schaefer, K. Morokuma), *Applied Quantum Chemistry*, Reidel, **1986**, pp. 155-184.

## Entry for the Table of Contents

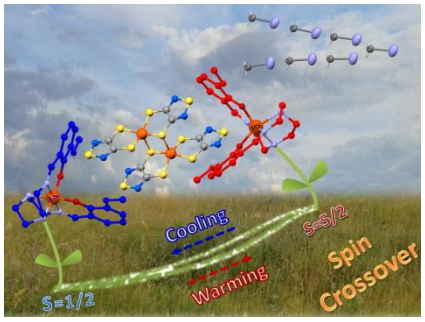


The fully characterized multi-magnetic salt [Fe(3-OMe-Sal$_2$trien)][Fe(tdas)$_2$]·CH$_3$CN shows a gradual thermally induced spin-crossover along with an antiferromagnetic exchange coupling in dimerized [Fe(tdas)$_2$]$_2^{2-}$ anions.

spin-crossover • iron(III) complexes • multi-magnetic salt • saltrien-type • 1,2,5-thiadiazole-3,4-dithiolate

URL: https://www.icp.ac.ru/

Twitter: @Nataliy074140.27